

# Uptake of HNO<sub>3</sub> to deliquescent sea-salt particles: a study using the short-lived radioactive isotope tracer <sup>13</sup>N

C. Guimbaud<sup>1</sup>, F. Arens<sup>1</sup>, L. Gutzwiller<sup>1</sup>, H. W. Gäggeler<sup>1,2</sup>, and M. Ammann<sup>1</sup>

<sup>1</sup>Paul Scherrer Institute, CH-5232 Villigen PSI, Switzerland

<sup>2</sup>Department of Chemistry and Biochemistry, University of Bern, CH-3012 Bern, Switzerland

Received: 8 April 2002 – Published in Atmos. Chem. Phys. Discuss.: 12 June 2002

Revised: 3 September 2002 – Accepted: 5 September 2002 – Published: 8 October 2002

**Abstract.** The uptake of HNO<sub>3</sub> to deliquescent airborne sea-salt particles (RH = 55%,  $P = 760$  torr,  $T = 300$  K) at concentrations from 2 to 575 ppbv is measured in an aerosol flow tube using <sup>13</sup>N as a tracer. Small particles ( $\approx 70$  nm diameter) are used in order to minimize the effect of diffusion in the gas phase on the mass transfer. Below 100 ppbv, an uptake coefficient ( $\gamma_{\text{upt}}$ ) of  $0.50 \pm 0.20$  is derived. At higher concentrations, the uptake coefficient decreases along with the consumption of aerosol chloride. Data interpretation is further supported by using the North American Aerosol Inorganics Model (AIM), which predicts the aqueous phase activities of ions and the gas-phase partial pressures of H<sub>2</sub>O, HNO<sub>3</sub>, and HCl at equilibrium for the NaCl/HNO<sub>3</sub>/H<sub>2</sub>O system. These simulations show that the low concentration data are obtained far from equilibrium, which implies that the uptake coefficient derived is equal to the mass accommodation coefficient under these conditions. The observed uptake coefficient can serve as input to modeling studies of atmospheric sea-salt aerosol chemistry. The main sea-salt aerosol burden in the marine atmosphere is represented by coarse mode particles ( $> 1 \mu\text{m}$  diameter). This implies that diffusion in the gas-phase is the limiting step to HNO<sub>3</sub> uptake until the sea-salt has been completely processed.

## 1 Introduction

Atmospheric oxidation of nitrogen oxide species (NO<sub>x</sub>) results mainly in the formation of HNO<sub>3</sub>, which is a major acidifying species in the troposphere. Heterogeneous loss to sea-salt aerosol has been suggested to play an important role in the removal pathway of nitrogen oxides in the marine tro-

posphere via the acid-displacement reaction (1) (Davies and Cox, 1998; Spokes et al., 2000).



Under most conditions in the marine troposphere, sea-salt aerosol is present in the form of deliquescent aerosol particles. However, the majority of laboratory experiments dealing with the HNO<sub>3</sub> sea-salt interaction performed to date have mainly provided kinetic information for NaCl exposed to HNO<sub>3</sub> in the form of solid thin-films or crystals. The measured rate of uptake was found to be very dependent on the humidity that the particles were exposed to prior and during the experiment (Beichert and Finlayson-Pitts, 1996; Davies and Cox, 1998; Ghosal and Hemminger, 1999). The main conclusion from these studies is that exposure to humidity leads to water adsorption at defect sites of the NaCl crystal lattice, followed by the formation of Cl<sup>-</sup> anions. Once such a local aqueous phase has been established, HNO<sub>3</sub> readily dissociates and the acid-displacement (1) can proceed. Indeed, Beichert and Finlayson-Pitts have observed that at high humidity, uptake of HNO<sub>3</sub> to crystalline NaCl films at 298 K led to a significant release of HCl in the gas-phase. The overall kinetics seems to be controlled by the dissociative adsorption process (Davies and Cox, 1998) into the adsorbed water. Scaled up to the case of fully dissolved (i.e. deliquesced) sea-salt particles, one might expect that the kinetics will be controlled by mass accommodation of HNO<sub>3</sub> as acid dissociation is known to be very fast in the aqueous phase. Therefore, to quantify the impact of this acid displacement under atmospheric conditions, one needs to measure the uptake of HNO<sub>3</sub> to deliquescent airborne sea-salt particles.

In a smog chamber experiment, Ten-Brink (1998) studied the ionic content (Cl<sup>-</sup> and NO<sub>3</sub><sup>-</sup>) of airborne NaCl particles during HNO<sub>3</sub> uptake. The presence of nitrate was accompanied by an equivalent loss of chloride from the particles. The authors found that the rate of substitution of chloride ions by nitrates is independent of the size of deliquescent

Correspondence to: C. Guimbaud  
(christophe.guimbaud@psi.ch)

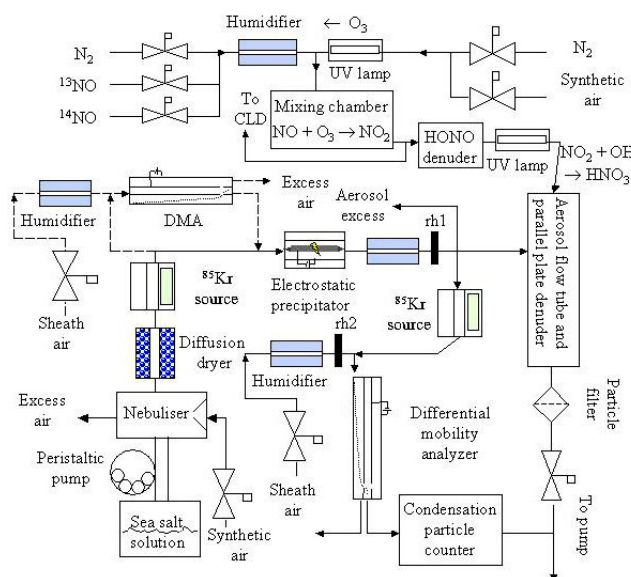


**Fig. 1.** Aerosol flow tube system and experimental set up to generate HNO<sub>3</sub> and sea-salt particles.

NaCl particles, and suggested that the rate-limiting step for reaction (1) is the formation or the release of HCl(g) and not nitric acid uptake to the particles. More recently, Abbatt and Waschewsky (1998) measured the uptake of HNO<sub>3</sub> to deliquescent NaCl particles at room temperature and atmospheric pressure using an aerosol flow tube. The authors reported a value of 0.2 as a lower limit to the uptake coefficient. The true uptake coefficient could not be derived because the mass transfer to the micrometer-sized particles was limited by diffusion in the gas phase. In addition, the dependence of the uptake coefficient on HNO<sub>3</sub> concentration was not investigated in detail.

In this work HNO<sub>3</sub> uptake to deliquescent airborne sea-salt particles (RH = 55%) is measured at HNO<sub>3</sub> concentrations ranging from 2 to 575 ppbv. Small particles ( $\approx 70$  nm diameter) are used in order to minimize the effects of gas-phase diffusion on the mass transfer. The effect of the gas-phase HNO<sub>3</sub> concentration on the measured uptake coefficient and on the distribution of HCl between the aerosol and the gas-phase will be discussed by an equilibrium thermodynamic model applied to the NaCl/HNO<sub>3</sub>/H<sub>2</sub>O system.

## 2 Experimental

The experimental techniques employed here are similar to those reported previously (Ammann, 2001; Kalberer et al., 1999). Nitrogen oxides labeled with the short-lived radioactive isotope <sup>13</sup>N are mixed with the aerosol particles in a flow reactor. Gas-phase and particulate products are trapped in denuders and in a filter, respectively, downstream of the reactor. The concentration of each gaseous and particulate species is

obtained by counting the number of decays of <sup>13</sup>N in each trap. The production of <sup>13</sup>N in the form of <sup>13</sup>NO has been described in detail elsewhere (Ammann, 2001). The experimental schematic to generate HNO<sub>3</sub> and the sea-salt particles is shown in Fig. 1, and described hereafter.

### 2.1 Production of HNO<sub>3</sub>

<sup>13</sup>N is transported as <sup>13</sup>NO in a carrier gas (He) to the chemistry laboratory through a capillary. A fraction of this <sup>13</sup>NO is mixed with the buffer gas (1 slpm of N<sub>2</sub>). In the majority of the experiments performed (except for uptake experiments at low ppb levels of HNO<sub>3</sub>) additional carrier <sup>14</sup>NO is added from a certified cylinder containing 10 ppm of NO in N<sub>2</sub> (using a calibrated mass flow controller), in order to provide total NO concentrations ranging from 1 ppbv to 1 ppmv. <sup>13</sup>NO and <sup>14</sup>NO (further designated as NO) are oxidized to <sup>13</sup>NO<sub>2</sub> and <sup>14</sup>NO<sub>2</sub> (further designated as NO<sub>2</sub>) by reaction with O<sub>3</sub> in a 2 liter flow reactor. Ozone is generated by diluting a small flow of synthetic air with N<sub>2</sub> and then passing it through a quartz tube irradiated by a Xe excimer lamp delivering UV light at 172 nm. The O<sub>3</sub> concentration is adjusted by varying the O<sub>2</sub>/N<sub>2</sub> mixing ratio and the light intensity, such that a minimum amount of O<sub>3</sub> is left after the complete conversion of NO to NO<sub>2</sub>. HNO<sub>3</sub> is produced from the reaction of NO<sub>2</sub> with OH radicals: the flow containing NO<sub>2</sub> is humidified to 40% relative humidity at 25°C and irradiated with 172 nm light in order to produce OH radicals. The hydroxyl radicals rapidly convert NO<sub>2</sub> into HNO<sub>3</sub> with yields ranging from 80–90%. The overall oxygen content is kept at a minimum in order to avoid O<sub>3</sub> concentrations larger than 100 ppbv after the second UV lamp. The O<sub>3</sub> concentration in the system should be kept low in order to maintain the high absorption efficiency of the denuders.

### 2.2 Production of the sea-salt particles

Sea-salt particles are produced by nebulising a solution of commercially available sea-salt (BIOMARIS®, BIOREX AG, Ebnat-Kappel, Switzerland) originating from the Atlantic Ocean. The elemental composition of the sea-salt used in these experiments has been analyzed by ion-chromatography. Cl<sup>-</sup> ions represent more than 97% of the total budget (molality) of the solvated anions (minor anions are, acetate, formate, and methane sulfonic acid). Cations are mainly represented by Na<sup>+</sup> (93%), with traces of Potassium (3%), Magnesium (3%) and Calcium (1%). Aerosol conditioning and characterization were described in detail by Wachsmuth et al. (2002). The sea-salt aerosol particles are initially humidified to a relative humidity (RH) of 75% to ensure that the particles are deliquescent before they are admitted to the flow tube where the final humidity is 55%. The humidity in the flow tube is kept below 75% in order to minimize the effect of HNO<sub>3</sub> retention on the walls. RH is measured using capacitance humidity sensors. The total aerosol

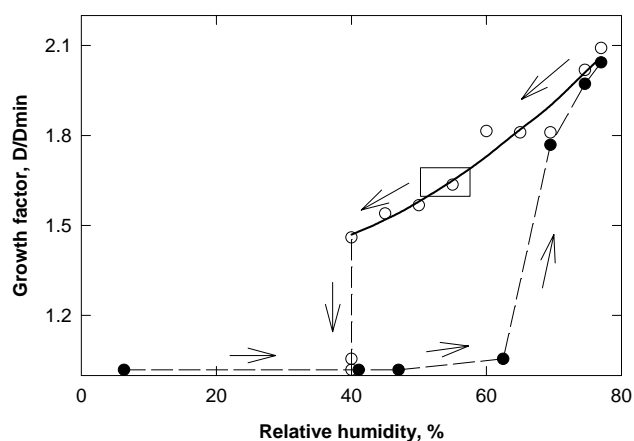


**Fig. 2.** Growth factors of BIOMARIS sea-salt particles as a function of relative humidity, at 294 K.  $D_{\min}$  is the diameter of average surface (45 nm) of the dry mono-disperse aerosol (RH = 6.3%). The experimental growth factor data have been sorted by increasing RH (filled circles) and by decreasing RH (empty circles). Increasing RH means that the mono-disperse aerosol has been exposed to the same RH after the first DMA and in the SMPS measurement system. When a RH value of about 70% is reached the particles become deliquescent (a solution droplet is formed), as shown by the jump in the growth curve (filled circles). Decreasing RH means that the mono-disperse aerosols have been deliquescent (exposed to a RH value of 75% after the first DMA) prior to being measured at a lower relative humidity in the SMPS system. The particle size decreases with decreasing humidity but the particles remain deliquescent until a RH value of almost 40% (empty circles). For deliquescent particles, a fitted curve of relative growth factors as a function of RH is presented, in order to estimate the decrease in size of the particle diameter at RH = 55% compared to particles formed at the DRH value of 70%. The rectangle area represents our experimental conditions, where HNO<sub>3</sub> uptake is measured.

surface to volume ratio in the flow tube is  $7 \times 10^{-5} \text{ cm}^2$  of aerosol per  $\text{cm}^3$  of air, with a variability of 10% (1  $\sigma$  precision). The determination of the total aerosol surface to volume ratio is critical for an accurate evaluation of the uptake coefficient, and is performed with a Scanning Mobility Particle Sizer (SMPS) consisting of a DMA (differential mobility analyser) and a condensation particle counter (CPC, TSI 3022). The same relative humidity is maintained in both the DMA sheath air and in the aerosol flow tube (RH = 55%) since the aerosol liquid water content and consequently the particle diameter and the aerosol surface to volume ratio are strongly dependent on the relative humidity.

Since the deliquescence properties of real sea-salt particles are not well documented and in order to ensure that the particles remained deliquescent under our experimental conditions (RH = 55%), we investigated the growth factors of our sea-salt particles as a function of the relative humidity. To achieve this, the poly-disperse dry aerosol is fed into an additional DMA delivering a mono-disperse aerosol ( $d_1 = 45 \text{ nm}$

diameter in average), as represented by the dashed lines path in Fig. 1. The mono-disperse aerosol is then neutralized, humidified at an initial RH value  $rh_1$ , and the resulting size ( $d_1$ ) of the dry/wet particles is measured at a second independent RH value  $rh_2$  with the SMPS system described earlier. The growth factor study of our marine sea-salt aerosol is presented and explained in Fig. 2. The purpose of this figure is not to determine with accuracy the Deliquescence Relative Humidity (DRH) and the Efflorescence Relative Humidity (ERH) values for our marine sea-salt aerosol but just to confirm that particles remain deliquescent (supersaturated) under our experimental conditions. Nevertheless, the growth factor of our marine sea-salt aerosol is discussed to assess the extent of supersaturation and to compare with the one observed for a pure NaCl aerosol. Indeed, in the increasing RH part of the curve (Fig. 2), where  $rh_1 = rh_2$ , the growth factor  $d_2/d_1$  jumps from 1 to 1.8–1.9 at a RH value of 70%. This RH value, which represents the deliquescence relative humidity, is slightly lower than the one observed by Tang et al. (1977) and by Gysel et al. (2002) for a pure NaCl aerosol at 298 K (DRH = 75%), whereas the growth factors observed are similar. The growth factor  $d_2/d_1$ , presented in the decreasing RH part of the curve (Fig. 2) where sea-salt particles are pre-humidified to  $rh_1 = 75\%$ , decreases continuously below the DRH value to reach 1.5–1.6 when the gas is dried to a  $rh_2$  value of 50–55%. Then, the growth factor drops to 1 when the gas is dried to an  $rh_2$  value of around 40% (ERH), meaning that crystallisation takes place. This continuous reduction in particle size, called hysteresis effect, is the result of the droplet becoming supersaturated and is very similar to the one observed for a pure NaCl aerosol. This implies that the particles are deliquescent and are supersaturated solutions under our experimental conditions for HNO<sub>3</sub> uptake measurements ( $rh_2 \approx 55\%$ ).

The average diameter of the particles is 70 nm (smaller than what is observed in the atmosphere) and the size distribution is lognormal. For aerosol flow tube experiments, the small particle size is more convenient because, (i) uptake of trace gas molecules is less affected by diffusion limitation and therefore practically proportional to the total surface area of the particles, and (ii) particles are less subject to impaction losses in a flow system.

Aerosol and HNO<sub>3</sub> flows are mixed in the aerosol flow tube. This flow tube consisted of a PFA Teflon tube of 8 mm inner and 10 mm outer diameter. HNO<sub>3</sub> is admitted through a 4 mm inner and 6 mm outer diameter PFA tube used as a sliding injector. This injector can be inserted until the end of the outer tube in order to determine HNO<sub>3</sub> loss to the walls without aerosol present (see below). The aerosol is introduced to the flow tube through a T-connector into the annular space between the injector and the flow tube. The flow tube assembly is held at room temperature. A new outer tube, cut to the length corresponding to the desired reaction time, is used for every experiment, because even though the number of sea-salt particles deposited on the walls is very low, they

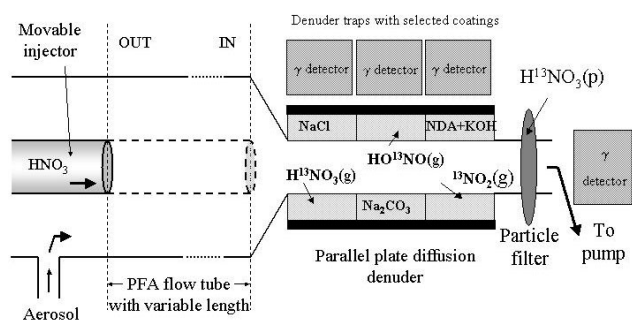


**Fig. 3.** Flow reactor and detection setup for gas phase molecules (NO<sub>2</sub>, HONO and HNO<sub>3</sub>) and for HNO<sub>3</sub> in particle phase (HNO<sub>3</sub>(p)).

still affect the loss rate of HNO<sub>3</sub> after some time.

### 2.3 The detection system and its calibration

After passing through the flow tube, the resulting flow enters a narrow parallel-plate diffusion denuder with selectively coated walls absorbing HNO<sub>3</sub>(g), HONO(g) and NO<sub>2</sub>(g), respectively, followed by a particle filter collecting the sea-salt particles with HNO<sub>3</sub>(p) and its products (Fig. 3). A small amount of HONO (several % relative to HNO<sub>3</sub>) is always produced from the reaction of OH with traces of NO during HNO<sub>3</sub> production. For HNO<sub>3</sub>, the walls of the first pair of denuder plates (10 cm long) are wetted with a saturated aqueous solution of NaCl and then dried in N<sub>2</sub>. For HONO, the second pair of denuder plate walls is wetted with a 1.4% solution of Na<sub>2</sub>CO<sub>3</sub> in 50% methanol/water and subsequently dried in N<sub>2</sub>. We note that also HCl released from the particles is absorbed on this section of the denuder. For NO<sub>2</sub>, the third pair of denuder plates (12 cm long) is coated with a solution of 1% NDA (*N*-(1-naphthyl) ethylenediamine dihydrochloride), 1% KOH and 10% water in methanol solution, and then dried in N<sub>2</sub> as well. In a denuder system, the gas passes in a laminar flow profile. The absorption of molecules capable of being taken up on the denuder plates is controlled by lateral diffusion, whereas the particles pass through the parallel plate denuder with close to 100% efficiency due to their very low diffusion coefficient. Under the present flow conditions, the characteristic time for this separation of HNO<sub>3</sub> from the aerosol is about 20 ms. The performance of this system has been demonstrated previously (Ammann, 2001). The HNO<sub>3</sub> uptake coefficient is derived from the concentration change of HNO<sub>3</sub> in the gas phase at the end of the flow tube when the aerosol was admitted to the flow tube, and from the concentration equivalent to HNO<sub>3</sub> taken up by the particles. At a given flow rate, these concentrations are obtained from the flux of <sup>13</sup>N-labeled molecules into the corresponding trap, *j*, multiplied by the ratio of labeled to non-labeled molecules. The concentration of non-labeled molecules is obtained using a chemiluminescence detector (see Fig. 1). The flux into

trap *j*, *I<sub>j</sub>*, is equal to the saturating activity at this trap and is derived from the difference between two consecutive activity measurements, *A<sub>j(i-1)</sub>* and *A<sub>j(i)</sub>*, recorded at times *t<sub>(i-1)</sub>* and *t<sub>(i)</sub>*. Each activity, *A<sub>j</sub>*, is recorded every 3 min with an integration time of 2 min, using a fixed  $\gamma$  detector. Fluxes, or saturating activities, are derived from Eq. (2), where  $\lambda$  is the decay constant of <sup>13</sup>N ( $\lambda = 0.00116 \text{ s}^{-1}$ ).

$$I_j = \frac{A_{j(i)} - A_{j(i-1)} e^{-\lambda(t(i)-t(i-1))}}{1 - e^{-\lambda(t(i)-t(i-1))}} \quad (2)$$

The relative counting efficiency of each  $\gamma$  detector is obtained by accumulating a certain amount of <sup>13</sup>NO<sub>2</sub> on a pair of denuder plates and then moving those plates in front of each detector. The activity recorded with each detector is corrected for the time elapsed since the end of the accumulation.

The narrow deposition pattern in each denuder has been well established (Ammann, 2001). It shows that the collection efficiency of the molecules is 100% on the denuders and on the filter. This is checked by regularly measuring the amount of <sup>13</sup>N absorbed on each trap with a scanning counting system described in Ammann (2001) that provides a spatial distribution of <sup>13</sup>N along the denuders.

## 3 Results

### 3.1 Observation of uptake in the flow tube

In the experiments, we measure a net first order loss rate of HNO<sub>3</sub> in the gas phase and use it to derive the uptake coefficient ( $\gamma_{\text{upt}}$ ). (see the next section for the definition of the terms and for the derivation procedure). Each value of  $\gamma_{\text{upt}}$  is obtained from individual experiments performed at a given HNO<sub>3</sub> concentration and reaction time. This is done according to the procedure described hereafter and presented in Figs. 3 and 4. For comparison purposes, typical records from experiments at both high and low HNO<sub>3</sub> concentration are shown in Fig. 4.

Initially, a new PFA flow tube is installed. The injector is introduced all the way inside the flow tube (position IN). The UV lamp generating HNO<sub>3</sub> is off, and no aerosol is introduced in the flow tube. A constant flow of NO<sub>2</sub> is established (NO<sub>2</sub>(g)<sub>IN</sub>). Switching on the UV light leads to a drop of the NO<sub>2</sub> signal and to an increase of the HNO<sub>3</sub> signal (HNO<sub>3</sub>(g)<sub>IN</sub>). Next, the injector is pulled out leading to a drop in the HNO<sub>3</sub> signal (HNO<sub>3</sub>(g)<sub>OUT</sub>), which is significant at low concentrations (Fig. 4, upper panel) and much less so at high concentrations (Fig. 4, lower panel). This observed drop is used to determine the wall loss rate. This apparent loss is caused by retention of HNO<sub>3</sub> on the flow tube walls due to reversible adsorption, and to the simultaneous decay of <sup>13</sup>N (not a true chemical loss process on the walls). Finally, the aerosol is introduced leading to another drop in the HNO<sub>3</sub> signal (HNO<sub>3</sub>(g)<sub>OUT,AER</sub>) and to an increase in

the signal on the filter from HNO<sub>3</sub> taken up by the particles (HNO<sub>3</sub>(p)<sub>OUT,AER</sub>). The reaction time for each experiment is given by the distance the injector is pulled out.

### 3.2 Derivation of the uptake coefficient

The uptake coefficient ( $\gamma_{\text{upt}}$ ) is defined according to the resistance model given by Hanson et al. (1994) and Hanson (1997).  $\gamma_{\text{upt}}$  is the probability that a molecule colliding with the particle surface is processed on or beyond the surface, i.e. the probability that the molecule is definitely lost from the gas phase. To clarify,  $\gamma_{\text{upt}}$  is not equal to  $\alpha$  (mass accommodation coefficient) which is the probability that a molecule loses its vertical kinetic energy after collision and is dissolving at the surface. Thus,  $\gamma_{\text{upt}}$  is expected to be smaller than  $\alpha$  as a dissolved molecule may also evaporate back to the gas phase.

From the observations made above, pseudo first order rate constants of H<sup>13</sup>NO<sub>3</sub> for wall loss ( $k_w$ ) and for uptake on the sea-salt aerosol ( $k_p$ ) are derived according to the relations (3) and (4), respectively, where  $\tau$  is the reaction time.

$$k_w = -\frac{1}{\tau} \ln \frac{[\text{HNO}_3(\text{g})_{\text{OUT}}]}{[\text{HNO}_3(\text{g})_{\text{IN}}]} \quad (3)$$

$$\frac{[\text{HNO}_3(\text{p})_{\text{OUT,AER}}]}{[\text{HNO}_3(\text{g})_{\text{IN}}]} = \frac{1 - e^{-(k_w+k_p)\tau}}{1 + \frac{k_w}{k_p}} \quad (4)$$

The first order loss rate constant in the gas phase ( $k_p$ ) is related to the net uptake coefficient ( $\gamma_{\text{net}}$ ) via Eq. (5), where  $S_p$  is the total surface of particles to volume ratio of air and  $v$  is the mean thermal velocity of HNO<sub>3</sub>:

$$k_p = \gamma_{\text{net}} S_p \frac{v}{4} \quad (5)$$

$\gamma_{\text{net}}$  is significantly different from  $\gamma_{\text{upt}}$  when the loss from the gas phase is affected by diffusion, usually expressed as in Eq. (6):

$$\frac{1}{\gamma_{\text{net}}} = \frac{1}{\Gamma_{\text{diff}}} + \frac{1}{\gamma_{\text{upt}}} \quad (6)$$

Using the approximate solution to this diffusion problem provided by Fuchs and Sutugin (1970), the diffusion correction ( $\Gamma_{\text{diff}}$ ) is given by Eq. (7), where  $Kn$  is the Knudsen number given by Eq. (8),  $\lambda$  is the mean free path of HNO<sub>3</sub> and  $d_p$  is the aerosol diameter:

$$\frac{1}{\Gamma_{\text{diff}}} = \frac{0.75 + 0.28 Kn}{Kn(1 + Kn)} \quad (7)$$

$$Kn = \frac{2\lambda}{d_p} \quad (8)$$

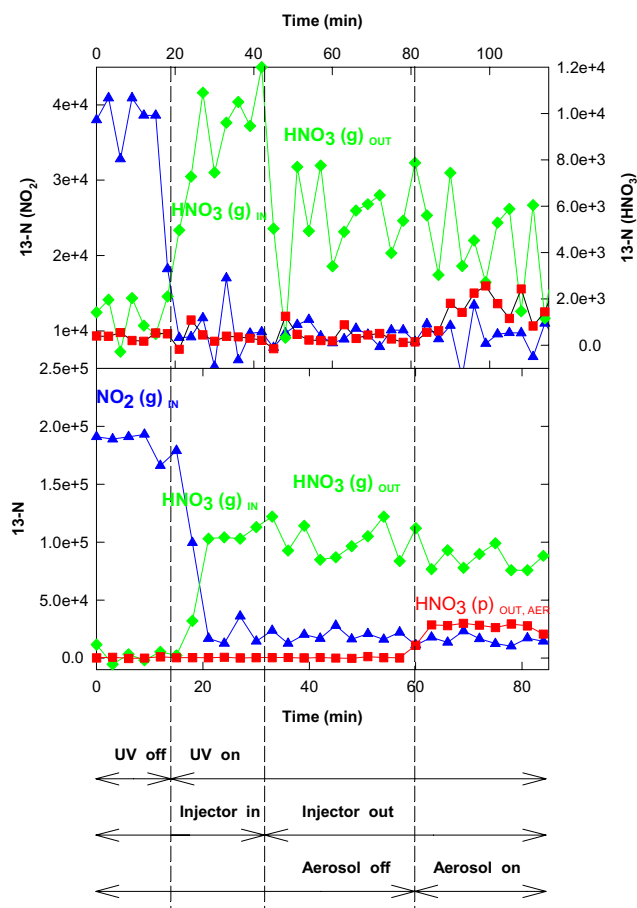


**Fig. 4.** On line records of HNO<sub>3</sub>(g) (green diamonds), NO<sub>2</sub>(g) (blue triangles), and HNO<sub>3</sub> attached to the particles (red squares) for a typical experiment performed at 9 ppbv (upper chart) and at 575 ppbv (lower chart) of HNO<sub>3</sub> present in the gas phase. Different time axis are presented for the two charts, in order to show the different steps of the protocol. Noteworthy, at low HNO<sub>3</sub> concentration (upper chart) the values are much more scattered, and thus a longer recording time is required to improve the statistics of the results. Also, at 9 ppbv of HNO<sub>3</sub> the relative decay of H<sup>13</sup>NO<sub>3</sub> due to retention on the wall is more significant (as seen from the difference of the HNO<sub>3</sub> signals between injector IN and OUT, but aerosol OFF).

### 3.3 Uptake coefficient of HNO<sub>3</sub>

Experiments are performed and evaluated as described above at HNO<sub>3</sub> concentrations ranging from 2 to 575 ppbv and at reaction times ranging from 0.2 to 2 s (obtained by using different flow tube lengths of 5 to 50 cm). From each of these individual experiments the average  $\gamma_{\text{upt}}$  derived are  $(0.55 \pm 0.14)$ ,  $(0.53 \pm 0.15)$ ,  $(0.41 \pm 0.10)$  and  $(0.36 \pm 0.09)$  for 2, 9, 57 and 575 ppbv of HNO<sub>3</sub> concentration, respectively (Fig. 5).

For the low HNO<sub>3</sub> concentrations (2, 9, and 57 ppbv), no dependence of  $\gamma_{\text{upt}}$  with the flow tube length is observed.

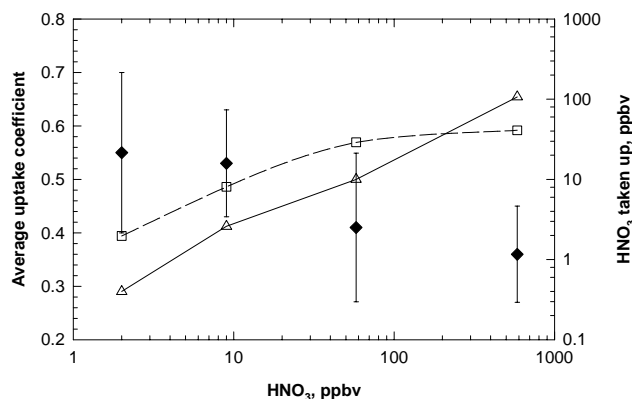


**Fig. 5.** Measured average uptake coefficient (plain diamonds) as a function of HNO<sub>3</sub> concentration (2, 9, 57 and 575 ppbv). HNO<sub>3</sub> taken up observed is shown for a representative reaction time of 0.7 s (empty triangles), corresponding to a flow reactor length of 20 cm. For comparison, HNO<sub>3</sub> taken up in the aerosol phase at equilibrium and derived from the AIM model is also shown (empty squares).

Thus, an average value of  $(0.50 \pm 0.13)$  for  $\gamma_{\text{upt}}$  is obtained from all the individual measurements performed at 2, 9, and 57 ppbv HNO<sub>3</sub> concentrations. The experimental scatters given above are the standard deviation of  $\gamma_{\text{upt}}$  values derived from individual experiments.

Final errors ( $1\sigma$ ) include both experimental scatter ( $\pm 25\%$ ) and systematic errors ( $\pm 30\%$ ), combined by the method of error propagation. The potential systematic error is dominated by the uncertainty of the total particle surface area to volume of air ratio ( $S_p$ ). Whereas the particle diameter can be determined to within 2% using the DMA, a much larger systematic error is assigned to the uncertainty of the particle number based on the CPC measurement. A  $\gamma_{\text{upt}}$  average value of  $(0.50 \pm 0.20)$  is then derived from the measurements performed at low HNO<sub>3</sub> concentrations (57 ppbv and below), including both systematic and experimental errors.

However, at higher concentrations (575 ppbv), a significant dependence of  $\gamma_{\text{upt}}$  with the flow tube length is observed. Since at this high concentration the wall loss rate was negligible (see also Fig. 4),  $\gamma_{\text{upt}}$  could be obtained from the incremental changes of the signals between two flow tube lengths. Therefore, one can express  $\gamma_{\text{upt}}$  as a function of the reaction time. The result, plotted in Fig. 6, clearly shows the decrease of  $\gamma_{\text{upt}}$  with reaction time at this high concentration.

The question arises whether the decrease of  $\gamma_{\text{upt}}$  is due to simple consumption of Cl<sup>-</sup> ions or due to other saturation effects. It is assumed that at the deliquescence point our sea-salt particles contain the same number of Cl<sup>-</sup> ions as a saturated solution of NaCl. At the deliquescent point, the total number of Cl atoms present in the system ( $N_{\text{Cl}}$ ), calculated from Eq. (9), is  $9.6 \times 10^{11}$  Cl atoms per cm<sup>3</sup> of air.

$$N_{\text{Cl}} = (C_{\text{AER}} A_V S_{\text{NaCl}} \rho) / (M_{\text{NaCl}}) \quad (9)$$

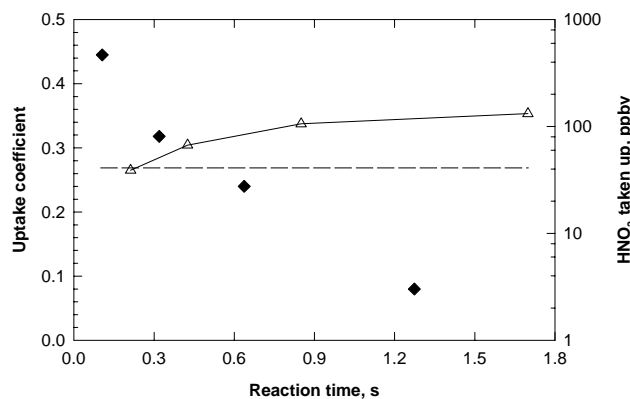


**Fig. 6.** Measured uptake coefficient (plain diamonds) as a function of reaction time, at 575 ppbv initial HNO<sub>3</sub> concentration. HNO<sub>3</sub> in the aerosol phase observed (empty triangles) and predicted at equilibrium (41 ppbv, horizontal line) are shown, assuming saturated sea-salt aerosols.

$C_{\text{AER}}$  is the aerosol volume concentration per cubic cm of air ( $3 \times 10^{-13}$  L cm<sup>-3</sup>),  $A_V$  the Avogadro number,  $S_{\text{NaCl}}$  the NaCl aqueous solubility at 25°C (0.26 g of NaCl per g of solution; Lorimer, 1991),  $\rho$  the density of a saturated aqueous solution of NaCl at 25°C (1200 g per liter of solution), and  $M_{\text{NaCl}}$  the molar mass of NaCl ( $58.5$  g mol<sup>-1</sup>). However, the particle diameter decreases by almost 20% between the deliquescence relative humidity (DRH) of 70% and the RH of 55% (Fig. 2). This is in line with observations on pure NaCl particles with a DRH of 75% (Tang et al., 1977; Gysel et al., 2002) and an about 15% decrease in diameter when the humidity is decreasing from 75% RH to 55% RH. This implies that in our experiment the particle volume decreases by almost 50% resulting in an about 100% super-saturation with respect to chloride. Therefore, the true chloride content was approximately  $2 \times 10^{12}$  Cl atoms per cm<sup>3</sup> at 55% RH. On the other hand, at 575 ppbv HNO<sub>3</sub> concentration and for a reaction distance of 10 cm in the flow tube, 11% of gas phase HNO<sub>3</sub> is observed to be taken up by the particles, corresponding to about 60 ppbv or  $1.5 \times 10^{12}$  molecules cm<sup>-3</sup> lost from the gas phase. Therefore, under these conditions, the number of HNO<sub>3</sub> molecules taken up is similar to the number of Cl atoms present in the sea-salt particles, and the decrease of  $\gamma_{\text{upt}}$  with reaction time seems to coincide with the complete displacement of chloride. Thus, as long as the sea-salt is not depleted of chloride,  $\gamma_{\text{upt}}$  is assumed to be independent of HNO<sub>3</sub> concentration and an average value of  $(0.50 \pm 0.20)$  is then derived from the data performed at low HNO<sub>3</sub> concentrations (from 2 to 57 ppbv). We note that from the measurements it seems that the fast uptake persists until complete consumption of chloride in the particles under our experimental conditions.

#### 4 Discussion

Based on the experiments, the uptake coefficient reported ( $\gamma_{\text{upt}} = 0.50 \pm 0.20$ ) is very high. In principle it is significantly different from 1.0 considering the conservative assessment of errors reported. We also note that the particle diameters are small enough so that the diffusion correction applied to the data is very small: the resistance term due to diffusion given by Eq. (7) ( $1/\Gamma_{\text{diff}} \approx 0.1$ ) is much smaller than the resistance term due to the uptake of HNO<sub>3</sub> ( $1/\gamma_{\text{upt}} = 2$ ). Thus, the uptake coefficient calculated ( $\gamma_{\text{upt}} = 0.50$ ) is very close to the net uptake coefficient derived from the loss rate ( $\gamma_{\text{net}} = 0.48$ ), according to the resistance model provided by Eq. (6).

$\gamma_{\text{upt}}$  is usually parameterized in the form (Hanson et al., 1994)

$$\frac{1}{\gamma_{\text{upt}}} = \frac{1}{\alpha} + \frac{1}{\Gamma_{\text{rxn}}} \quad (10)$$

where  $\frac{1}{\Gamma_{\text{rxn}}}$  denotes the resistance due to reaction, which is given by the removal rate of HNO<sub>3</sub> in the aqueous aerosol phase, until the system approaches equilibrium. The collision rate of HNO<sub>3</sub> (at 10 ppbv) with the surface of 70 nm diameter particles is on the order of  $10^5 \text{ s}^{-1}$ . Once dissolved, we assume that the first order rate constants for dissociation and protonation are faster than this by several orders of magnitude. The inverse of the characteristic time for diffusion across the particles is about  $10^7 \text{ s}^{-1}$ . The rate of thermal desorption of HCl from acidic surfaces is also at least  $10^7 \text{ s}^{-1}$  at room temperature (Morris et al., 2000). This means that the rate limiting step of uptake is mass accommodation (given by  $\alpha$ ), i.e. adsorption and solvation at the interface, unless equilibrium with respect to either HNO<sub>3</sub> or HCl is reached.

In what follows, we simulate the distribution of each species, i.e. HNO<sub>3</sub>(g), H(aq), Cl(aq), NO<sub>3</sub>(aq), and HCl(g) present at equilibrium for a NaCl-H<sub>2</sub>O-HNO<sub>3</sub> system for HNO<sub>3</sub> concentrations ranging from 2 to 575 ppbv representative of our aerosol experiment. The purpose is (i) to determine how far from equilibrium each  $\gamma_{\text{upt}}$  measurement is performed and (ii) to assess whether at high HNO<sub>3</sub> concentration (575 ppbv) still all or almost all Cl(aq) can be released into the gas phase as HCl. We used the North American Aerosol Inorganics Model (AIM), made available on the internet (<http://mae.ucdavis.edu/wexler/aim.html>) where a short description of this model is presented (Clegg et al., 2000). The AIM contains a module for the system H<sup>+</sup>-NH<sub>4</sub><sup>+</sup>-Na<sup>+</sup>-SO<sub>4</sub><sup>2-</sup>-NO<sub>3</sub><sup>-</sup>-Cl<sup>-</sup>-H<sub>2</sub>O, originally described by Clegg et al. (1998). This part of the AIM predicts aqueous phase activities of each ion, equilibrium partial pressures of H<sub>2</sub>O, HNO<sub>3</sub>, HCl, NH<sub>3</sub> and H<sub>2</sub>SO<sub>4</sub>, and saturation with respect to nineteen solid phases, all at equilibrium.

Activity calculations for water and ions present in the aqueous aerosol, the most critical part of the model, utilize the Pitzer and Simonson (1986) and Clegg (1992) equations.

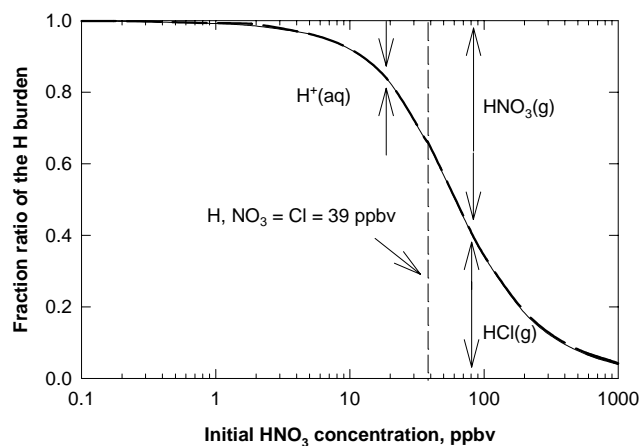


**Fig. 7.** Simulated distribution of the hydrogen burden for a NaCl-H<sub>2</sub>O-HNO<sub>3</sub> system representative of our aerosol experiment, at equilibrium, as a function of H and NO<sub>3</sub> inputs. The 39.2 ppbv input for H and NO<sub>3</sub> (vertical dashed line) is equal to the total amount of Cl present in the system, assuming saturated sea-salt aerosols.

The equilibrium state of the system is solved by Gibbs energy minimization. The model is developed for strong electrolytes and assumes complete dissociation of strong volatile acids in aqueous solution. The thermodynamic properties of the system are represented at concentrations up to saturation (with respect to the solid phases). The model input includes ambient relative humidity (expressed as a fraction) and the total number of each “ion” and water molecules introduced in the system (expressed in mole per cubic meter of air). The “ions” are hydrogen, ammonium, sodium, sulphate, nitrate and chloride. Each “ion” can equilibrate within 3 phases, i.e. either as true ion in the aqueous phase, as a salt in the solid phase, or as an acid in the gas phase. The temperature is 298.15 K.

The model output provides the amounts of liquid water, dissolved ions, and solids present at equilibrium, expressed in terms of molecules per cubic meter of air and in molality (mole per kg of water). The partial pressures of gas-phase species present as HCl, HNO<sub>3</sub>, NH<sub>3</sub>, or H<sub>2</sub>SO<sub>4</sub> that would be in equilibrium with the condensed phase are also reported.

Because the model cannot treat supersaturated solutions, the calculations were performed at the deliquescence point. Then, the total number of sodium and chloride present in our aerosol system is  $1.60 \times 10^{-6} \text{ mol m}^{-3}$  of air. This number is derived from the  $N_{\text{Cl}}$  value of  $9.6 \times 10^{11} \text{ Cl atoms cm}^{-3}$  calculated in the results section from the aerosol volume. The relative humidity is set to a value between 0.7 and 0.8 in order to maintain an amount of liquid water of  $1.46 \times 10^{-5} \text{ mol m}^{-3}$  of air, equivalent to the estimated one in our aerosol experiments.

Figure 7 simulates the distribution of the hydrogen species present at equilibrium in the different molecular states as a function of the initial HNO<sub>3</sub> concentration in the flow reac-

tor. For low initial HNO<sub>3</sub>(g) concentrations (2 ppbv or less), more than 98% of the HNO<sub>3</sub>(g) is taken up in the aqueous phase and is displaced as HCl into the gas phase when equilibrium is reached. The fraction of initial HNO<sub>3</sub>(g) displaced into HCl(g) remains even significant (almost 70%) when the amount of HNO<sub>3</sub> introduced is equal to the amount of Cl present in the system (expressed as 39.2 ppbv at 1 atm and 298 K), which is, as mentioned in the results section, lower than the true value for the supersaturated aerosol of the experiment. The result from this model is consistent with earlier model results on the HNO<sub>3</sub> sea-salt system (Brimblecombe and Clegg, 1988) reported for low HNO<sub>3</sub>/Cl ratios representative of the marine boundary layer. For 575 ppbv HNO<sub>3</sub> initial gas-phase concentration, the model shows that (i) 41 ppbv of HNO<sub>3</sub> is transferred to the aerosol phase at equilibrium and (ii) almost all the Cl ions initially present in the aqueous phase (39.2 ppbv equivalent) are displaced to the gas phase as HCl (38.5 ppbv) at equilibrium.

When comparing the model results with the experimental data, we assume that the model trends can simply be extrapolated to the supersaturated solution, i.e. the main effect of the activity coefficients for supersaturated solutions is continuing to lead to strong displacement of HCl to the gas-phase compared to saturated solutions. We then expect that at 575 ppbv HNO<sub>3</sub>(g) still practically all Cl ions initially present in the aqueous phase are released to the gas-phase. In addition to the observed average uptake coefficients, Fig. 5 demonstrates that the observed amount of HNO<sub>3</sub> taken up for a reaction distance of 20 cm (i.e. a reaction time of 1 s) remains far from the amount of HNO<sub>3</sub> expected to be taken up at equilibrium, for the experiments performed at 2, 9, and 57 ppbv of HNO<sub>3</sub> gas-phase concentration. However, this is not the case for the experimental data obtained at 575 ppbv of HNO<sub>3</sub> gas-phase concentration. At 575 ppbv, the observed amount of HNO<sub>3</sub> taken up (106 ppbv) is in reasonable agreement with the model expectation (82 ppbv) when 100% supersaturation (doubled Cl content relative to saturation) is considered for the aerosol in our experiment. The model calculations imply that the equilibrium is only affecting the rate of uptake when the gas-phase concentration of HNO<sub>3</sub> significantly exceeds that of aerosol chloride and that even under these conditions all chloride is displaced into the gas phase as HCl. Therefore, the observed decrease of  $\gamma_{\text{upt}}$  with increasing reaction time (Fig. 6) goes directly along with chloride consumption. It also seems likely that the uptake remains limited by mass accommodation until the aerosol chloride starts to be significantly depleted.

## 5 Conclusions and atmospheric implications

The HNO<sub>3</sub> uptake coefficient on the submicron deliquescent sea-salt aerosol of our experiments is measured to be  $(0.50 \pm 0.20)$ . Primarily due to the high ionic strength of the salt solution, all HNO<sub>3</sub> taken up is readily displaced as HCl

into the gas-phase. Since all processes in the liquid phase (dissociation, protonation, diffusion) are faster than the rate of uptake at low HNO<sub>3</sub> concentrations, the measured uptake coefficient is likely to be equal to the mass accommodation coefficient. Such a high mass accommodation coefficient seems to be reasonable for soluble species. Our result confirms the only previous study performed in a flow tube reactor with deliquescent NaCl particles (Abbatt et al., 1998), where a lower limit of 0.2 was reported for the uptake coefficient. It is also in agreement with findings on solid NaCl surfaces exposed to HNO<sub>3</sub> and humidity, where the reaction rate scaled with the degree of solvation of chloride into adsorbed water at defect sites (Davies and Cox, 1998; Ghosal and Hemminger, 1999) and rapid release of HCl was observed (Beichert and Finlayson-Pitts, 1996). The observed decrease of the uptake coefficient observed at high HNO<sub>3</sub> concentration goes clearly along with the complete processing of available chloride, and is not due to incomplete dissociation of HNO<sub>3</sub> or incomplete displacement of HCl to the gas-phase.

Thus, an HNO<sub>3</sub> uptake coefficient of 0.5 is a representative input value for modeling studies of marine air masses with relatively clean sea-salt aerosol not yet affected by organic coatings etc. Also, this high uptake coefficient persists until all aerosol chloride is displaced into the gas phase as HCl. Nevertheless, in the marine boundary layer, the sea-salt aerosol burden is mainly represented by coarse mode particles ( $> 1 \mu\text{m}$  diameter) implying that the limiting factor for the HNO<sub>3</sub> transfer to the marine aerosol is not the reaction kinetics or diffusion in the bulk but rather the diffusion in the gas phase.

*Acknowledgements.* Valuable technical support was provided by E. Rössler, D. Piguet and M. Birrer by providing favourable conditions to perform this experiment. We gratefully acknowledge the staff of the PSI accelerator facilities for supplying stable proton beams over many days and nights. This work was supported by the Swiss National Science Foundation.

## References

- Abbatt, J. P. D., and Waschewsky, G. C. G.: Heterogeneous interactions of HOBr, HNO<sub>3</sub>, O<sub>3</sub>, and NO<sub>2</sub> with deliquescent NaCl aerosols at room temperature, *J. Phys. Chem. A*, 102, 3719–3725, 1998.
- Ammann, M.: Using <sup>13</sup>N as tracer in heterogeneous atmospheric chemistry experiments, *Radiochim. Acta*, 89, 831–838, 2001.
- Beichert, P. and Finlayson-Pitts, B. J.: Knudsen cell studies of the uptake of gaseous HNO<sub>3</sub> and other oxides of nitrogen on solid NaCl: The role of surface-adsorbed water, *J. Phys. Chem. A*, 100, 15 218–15 228, 1996.
- Brimblecombe, P. and Clegg, S. L.: The solubility and behaviour of acid gases in the marine aerosol, *J. Atmos. Chem.*, 7, 1–18, 1988.
- Clegg, S. L., Pitzer, K. S., and Brimblecombe, P.: Thermodynamics of multicomponent, miscible, ionic solutions. II. Mixtures including unsymmetrical electrolytes, *J. Phys. Chem. A*, 96, 9470–9479, 1992.



- Clegg, S. L., Brimblecombe, P., and Wexler, A. S.: A thermodynamic model of the system H-NH<sub>4</sub>-Na-SO<sub>4</sub>-NO<sub>3</sub>-Cl<sup>-</sup>-H<sub>2</sub>O at 298.15 K, *J. Phys. Chem. A*, 102, 2155–2171, 1998.
- Clegg, S. L., Brimblecombe P., and Wexler, A. S.: On-line aerosol inorganics model, <http://mae.ucdavis.edu/wexler/aim.html>, updated version of 6 September, 2000.
- Davies, J. A. and Cox, R. A.: Kinetics of the heterogeneous reaction of HNO<sub>3</sub> with NaCl: Effect of water vapor, *J. Phys. Chem. A*, 102, 7631–7642, 1998.
- Fuchs, N. A. and Sutugin, A. G.: Highly dispersed aerosols, Ann Arbor Science Publishers Inc., Ann Arbor London, 1970.
- Ghosal, S. and Hemminger, J. C.: Effect of water on the HNO<sub>3</sub> pressure dependence of the reaction between gas-phase HNO<sub>3</sub> and NaCl surfaces, *J. Phys. Chem. A*, 103, 4777–4781, 1999.
- Gysel, M., Weingartner, E., and Baltensperger, U.: Hygroscopicity of aerosol particles at low temperatures. Part II: Theoretical and experimental hygroscopic properties of laboratory generated aerosols, *Environ. Sci. Technol.*, 36, 63–68, 2002.
- Hanson, D. R., Ravishankara, A. R., and Solomon, S.: Heterogeneous reactions in sulfuric acid aerosols: a framework for model calculations, *J. Geophys. Res.*, 99, 3615–3629, 1994.
- Hanson, D. R.: Surface specific reactions on liquids, *J. Phys. Chem. B*, 101, 4998–5001, 1997.
- Kalberer, M., Ammann, M., Arens, F., Gäggeler, H. W., and Baltensperger U.: Heterogeneous formation of nitrous acid (HONO) on soot aerosol particles, *J. Geophys. Res.*, 104, 13 825–13 832, 1999.
- Lorimer, J. W.: Alkali metal and ammonium chlorides in water and heavy water (binary systems), Solubility data series, Vol. 47, (Ed) Cohen-Adad, R., Pergamon press, Oxford, 1991.
- Morris, J. R., Behr, P., Antman, M. D., Ringeisen, B. R., Splan, J., and Nathanson, G.: Molecular beam scattering from super-cooled sulfuric acid: collisions of HCl, HBr, and HNO<sub>3</sub> with 70 wt D<sub>2</sub>SO<sub>4</sub>, *J. Phys. Chem. A*, 104, 6738–6751, 2000.
- Pitzer, K. S. and Simonson, J. M.: Thermodynamics of multicomponent, miscible, ionic systems: theory and equations, *J. Phys. Chem. A*, 90, 3005–3009, 1986.
- Spokes, L. J., Yeatman, S. G., Cornell, S. E., and Jickells, T. D.: Nitrogen deposition to the eastern Atlantic Ocean. The importance of south-easterly flow, *Tellus B*, 52, 37–49, 2000.
- Ten-Brink, H. M.: Reactive uptake of HNO<sub>3</sub> and H<sub>2</sub>SO<sub>4</sub> in sea-salt (NaCl) particles, *J. Aerosol. Sci.*, 29, 57–64, 1998.
- Tang, I. N., Munkelwitz, H. R., and Davis, J. G.: Aerosol growth studies – II. Preparation and growth measurements of monodisperse salt aerosols, *J. Aerosol. Sci.*, 8, 149–159, 1977.
- Wachsmuth, M., Gäggeler, H. W., Von Glasow, R., and Ammann, M.: Accommodation coefficient of HOBr on deliquescent sodium bromide aerosol particles, *Atmos. Chem. Phys.*, 2, 121–131, 2002.